THE ASTROPHYSICAL JOURNAL, 223:840–853, 1978 August 1

THE DETAILED STRUCTURE OF CO IN MOLECULAR CLOUD COMPLEXES. II. THE W75–DR 21 REGION

JOHN R. DICKEL AND HÉLÈNE R. DICKEL
University of Illinois Observatory; and Sterrewacht, Leiden
AND
WILLIAM J. WILSON
Ivan A. Getting Laboratories, Aerospace Corporation
Received 1977 November 10; accepted 1978 February 8

ABSTRACT

Analysis of ^{12}CO and ^{13}CO spectral-line maps of the DR 21–W75 complex has revealed the presence of two large molecular clouds, one at a radial velocity of -3 km s^{-1} and the other at an average velocity near $+9$ km s^{-1}. Recognition of features common to both velocities suggests that the two clouds are interacting. The line profiles of the -3 km s^{-1} component exhibit a broad wing structure at all positions across the cloud, which has a radius greater than 10 pc. This is the first reported case of such wide wings on the CO line over an extended area of the sky. Comparison of the profiles with model calculations suggests that this cloud may be in overall gravitational collapse. The compact H II region DR 21 and several other condensations are embedded in this cloud, and the CO exhibits peaks at these sources. The $+9$ km s^{-1} cloud is less dense and shows a gradient in radial velocity across its face that is possibly caused by a differential retardation as it passes around the edge of the other component. The faint, compact H II region W75 N lies in this $+9$ km s^{-1} cloud.

Subject headings: interstellar: matter — interstellar: molecules — nebulae: individual

I. INTRODUCTION

The compact H II region DR 21 (Downes and Rinehart 1966) is part of a large complex which includes several other radio sources—e.g., a separate OH source DR 21(OH) (Goss 1968) and another faint continuum source W75 N with an associated OH maser (Wynn-Williams 1971). There is strong infrared emission at these positions and line emission from many interstellar molecules throughout the complex. The CO and other molecular emission generally appears at two radial velocities: -3 km s^{-1} and near $+9$ km s^{-1} (see, e.g., Wilson *et al.* 1974; Morris *et al.* 1974). To understand the detailed relationship of these features at the two different velocities, high-resolution maps of this complex in the $J = 1$–0 transition of both ^{12}CO and ^{13}CO were obtained using the 11 m telescope of NRAO. The CO is present everywhere in the complex at both velocities. Analysis of the line profiles throughout the region has allowed development of a tentative model of its structure and dynamics. The general picture requires two large interacting clouds containing individual excitation centers. In § II the observations are described, in § III the data and model are discussed, and in § IV a summary is presented.

II. OBSERVATIONS

The equipment and observing procedure used for these observations were described in Paper I of this series (Dickel, Dickel, and Wilson 1977) and shall be mentioned only briefly here. Some preliminary data were obtained in 1973, when the 11 m telescope was equipped with a mixer receiver having a receiver noise temperature of about 1500 K; however, most of the data were taken in 1974, when there was a cooled mixer receiver having a receiver noise temperature of about 600 K. Both 100 and 250 kHz filters were used in the spectrometer, which gave resolutions of 0.26 and 0.65 km s^{-1} or 0.27 and 0.67 km s^{-1} at ^{12}CO or ^{13}CO, respectively. A typical integration of 6 minutes gave an rms noise of 0.4 K and 0.2 K at ^{12}CO and ^{13}CO, respectively, for the 250 kHz data. These, and all temperatures given throughout this paper, are corrected antenna temperatures outside the atmosphere T_A^*; they are related to brightness temperatures by the forward beam efficiency, which is greater than or equal to 0.9 (Ulich and Haas 1976). Absolute calibration was provided by measurements of the CO emission from Orion A, for which antenna temperatures outside the atmosphere of 60 K and 9.3 K were assumed for ^{12}CO and ^{13}CO, respectively (Ulich and Haas 1976).

The data consisted of CO spectra obtained at fixed points on a grid spaced by 1′ around the three sources DR 21, DR 21(OH), and W75 N and with a larger spacing in other areas. Observations at the positions of DR 21 were repeated about once every hour to allow determination of the variable extinction coefficient, and then the antenna temperature at each position was corrected for the atmosphere at the time of observation.

Examination of the spectra has revealed that no

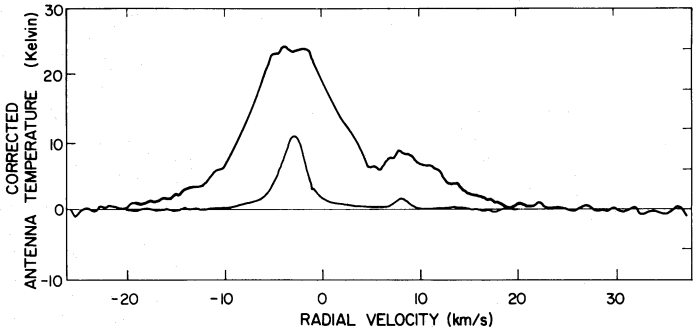

FIG. 1*a*

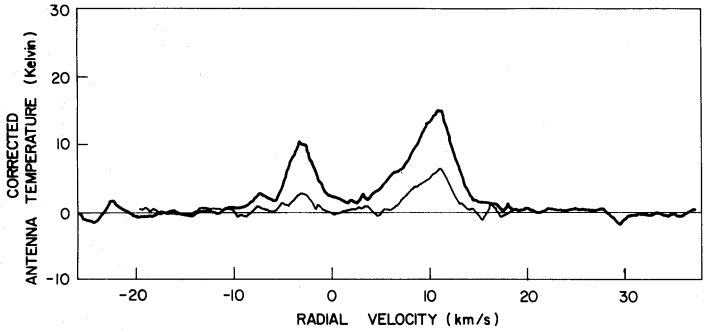

FIG. 1*b*

FIG. 1.—(*a*) Spectra of the ^{12}CO and ^{13}CO emission in the direction of DR 21 with a velocity resolution of ~ 0.65 km s^{-1} and 0.67 km s^{-1}, respectively. (*b*) Spectra in the direction of W75 N (position N19W20).

features are present with half-widths smaller than about 3 km s^{-1}. Therefore, in our analysis we have used data from the 250 kHz filters with their smaller noise level and also greater total bandwidth. The large bandwidth enabled us to study the details of a broad winglike structure as shown on the line centered near -3 km s^{-1} in the sample profile toward DR 21 in Figure 1*a*, with 250 kHz resolution. Figure 1*b* shows the profile toward W75 N. All the data clearly show the presence everywhere of the two components at -3 and $+9$ km s^{-1} and also the wings on the -3 km s^{-1} component. In Table 1 we present the parameters of both the ^{12}CO and ^{13}CO lines which have been fitted to the data at each position in the sky for the -3 km s^{-1} component, and in Table 2 we give the same data for the $+9$ km s^{-1} component. Columns (1) and (2) of both tables give the position relative to the center of DR 21 at $\alpha = 20^h37^m13^s$ and $\delta = 42°09'$ (1950). A dagger indicates data taken in 1973 with the lower signal-to-noise ratio. Columns (3)–(6) contain the peak corrected antenna temperature T_A^*, the central velocity V_c, the half-power width (in km s^{-1}) ΔV, and the integrated flux $T_A^* \Delta V$ of the ^{12}CO lines. For the -3 km s^{-1} component, the integrated flux does not include the power in the wings, which appear to deviate from and extend well above the fit of a Gaussian profile at a level below about 1/10 of the peak T_A^*. Column (7) of Table 1 gives the total velocity width of this broad wing structure between points where it reaches the baseline. The $+9$ km s^{-1} component is contaminated by the wing of the lower-velocity feature; to obtain the parameters in Table 2, Gaussians were fitted to the data after subtraction of the contribution from the other component. Columns (8)–(11) of Table 1 and (7)–(10) of Table 2 contain the parameters of the ^{13}CO lines for each component; columns (12) of Table 1 and (11) of Table 2 give the difference between the central velocities of the ^{12}CO and ^{13}CO components in terms of $V_c(^{12}CO)$ minus $V_c(^{13}CO)$. Next are given the ratios of the fitted parameters of the peak T_A^*, integrated flux, and half-power width for the ^{13}CO lines relative to the ^{12}CO lines at each position; finally, notes on the particular profiles are given in the last column of Tables 1 and 2. Contour maps of the distribution of these various parameters are presented in Figures 2–7 and in Figure 9; they will be described below.

III. DISCUSSION OF DATA AND MODEL

a) Extended Clouds

i) *General Properties*

The most obvious feature of the CO profiles in the direction of W75 is the presence of two distinct lines: a bright one with a central velocity of -3 km s^{-1} and a less intense one at $+9$ km s^{-1}. The bright feature at -3 km s^{-1} is strongest in the direction of DR 21 but

TABLE 1

OBSERVATIONAL PARAMETERS FOR THE CO IN THE -3 km s^{-1} COMPONENT OF THE DR 21–W75 COMPLEX

POSITION FROM CENTER‡		^{12}CO					^{13}CO				$V_{12}-V_{13}$	RATIOS ^{13}CO/^{12}CO			NOTES
		line parameters				width at base of wings	line parameters								
$\Delta\alpha$	$\Delta\delta$	T_A^*	V_C	ΔV	$T_A^*\Delta V$		T_A^*	V_C	ΔV	$T_A^*\Delta V$		T_A^*	$T_A^*\cdot\Delta V$	ΔV	
s	arcmin	K	km/s	km/s	K·km/s	km/s	K	km/s	km/s	K·km/s	km/s				
†W40	N00	12.9	-1.9	2.0	26	16									
†W40	N08	1.8	-3.0	5.0	9	--									1 MHz filters
†W40	N16	7.6	-2.3	3.9	30	26	<0.9					<.1			
†W40	N24	15.1	-2.5	4.0	60	34									
W30	N18	15.7	-2.3	4.8	75	25									
W30	N19	11.6	-2.9	2.6	30	14									
W30	N20	13.5	-3.4	2.5	34	17									
W25	N17	15.6	-2.6	3.9	61	27	3.1	-2.5	3.3	10	-0.1	.20	0.17	0.85	
W25	N18	14.0	-2.8	4.8	67	28	2.6	-3.2	2.9	8	0.4	.25	.11	.60	
W25	N19	10.9	-3.0	2.8	30	28									
†W20	S04	5.8	-3.0	4.5	26	20									
†W20	N00	18.3	-2.4	4.3	79	18	4.4	-1.9	3.9	17	-0.5	.30	.22	.91	
†W20	N04	15.4	-2.6	2.4	37	18	5.0	-3.2	5.4	27	0.6	.32	.73	2.27	very noisy
†W20	N08	15.0	-3.4	3.3	50	8	4.5	-3.2	3.3	15	-0.2	.30	.30	1.00	
†W20	N12	15.5	-3.5	2.8	43	16									
†W20	N16	(12.3)	-3.4	1.9	23	4									
W20	N17	18.1	-3.3	3.4	62	13									
W20	N18	13.5	-2.4	5.0	68	27	3.3	-2.2	3.7	12	-0.2	.30	.18	.74	
W20	N19	9.3	-2.0	4.8	45	32	1.9	-2.8	2.2	4	0.8	.20	.09	.46	
†W20	N20	10.5	-3.7	2.6	27	10									
W15	N17	14.3	-3.2	2.6	37	22									
W15	N20	9.7	-2.8	2.7	26	26									
W10	S01	21.5	-2.7	4.4	95	35	4.0	-2.5	3.0	12	-0.2	.24	.13	.68	
W10	N01	19.7	-2.4	4.8	95	37	3.7	-2.8	2.9	11	-0.4	.21	.11	.60	
†W10	N02	26.9	-3.2	3.5	94	28									
W10	N03	19.8	-2.6	4.2	83	27									
W10	N05	20.8	-2.8	4.6	96	14									
†W10	N06	19.7	-3.5	5.4	106	30									
W10	N14	19.3	-3.2	3.5	68	26									
W10	N14	13.2	-2.4	2.5	33	21									
W08	N18						<2.5								
W05	S02	20.2	-2.7	4.4	89	35	4.4	-2.	2.5	11	-0.7	.29	0.12	.57	
W05	S01	24.6	-3.0	7.4	182	34	5.6	-2.8	4.	22	0.2	.28	0.12	.54	
W05	N00	24.6	-3.1	9.8	241	34	6.8	-2.5	2.4	16	-0.6	.33	0.07	.25	
W05	N01	25.8	-2.6	5.5	142	33	5.7	-3.	3.	17	0.4	.26	0.12	.55	
W05	N02	25.8	-3.1	4.6	119	30	6.3	-3.	2.5	16	-0.1	.30	0.13	.54	
W05	N03	26.9	-3.0	5.8	156	28	5.6	-3.	2.5	14	0	.20	0.09	.43	
W05	N04	23.5	-2.9	6.8	160	30	6.5	-3.	3.5	22	0.1	.43	0.14	.52	
W05	N05	22.0	-2.9	5.6	123	30	8.0	-3.	3.	24	0.1	.41	0.19	.53	
†E00	S08	5.0	-3.2	8.4	42	32									
†E00	S04	9.7	-3.4	3.3	32	18									complex
E00	S01	23.4	-3.0	7.9	185	38	8.7	-2.5	3.5	30	-0.5	.49	0.16	.44	
‡E00	N00	24.5	-2.5	10.8	265	39	11.0	-2.5	3.2	35	0	.46	0.13	.30	
E00	N01	24.8	-2.7	6.2	154	31	8.9	-2.5	3.	27	-0.2	.37	0.17	.48	
E00	N02	25.2	-3.5	6.2	156	33	10.6	-3.	3.	32	-0.5	.44	0.20	.48	
E00	N03	26.4	-3.2	7.4	195	36	11.0	-3.	3.5	38	-0.2	.44	0.20	.47	
E00	N04	22.1	-3.3	7.6	168	29	10.1	-3.	4.	40	-0.3	.52	0.24	.53	
E00	N05	21.0	-3.3	6.8	143	39	10.4	-3.	4.	42	-0.3	.49	0.29	.59	
†E00	N08	19.9	-2.7	5.3	105	34	9.6	-2.1	3.0	29	-0.6	.50	0.27	.56	
†E00	N12	12.5	-1.6	3.0	38	28	4.9	-1.5	2.7	13	-0.1	.39	0.35	.90	
†E00	N16	7.6	-0.2	2.7	20	34	< .5					<.07			
†E00	N20	2.2	-4.2	5.4	112	24									
†E00	N24	4.8	-1.9	4.5	22	34									
E05	S02	20.5	-3.0	5.0	102	34	7.3	-3.	2.5	18	0	.39	0.18	.50	
E05	S01	23.4	-3.3	9.0	211	33	8.7	-2.5	3.	26	-0.8	.45	0.12	.33	
E05	N00	24.0	-3.2	8.5	204	38	7.5	-2.5	3.5	26	-0.7	.34	0.13	.41	
E05	N01	24.0	-3.2	6.0	144	36	7.8	-3.	3.2	25	-0.2	.40	0.17	.53	
E05	N02	25.8	-3.5	6.0	155	37	8.2	-3.	3.	25	-0.5	.37	0.16	.50	
E05	N03	25.2	-3.5	7.0	176	33	7.8	-3.	3.	23	-0.5	.37	0.13	.43	
E05	N04	23.4	-3.4	5.9	138	33	8.2	-3.	2.5	20	-0.4	.39	0.15	.42	
E05	N05	22.8	-4.3	6.8	155	33	8.2	-3.5	3.	25	-0.8	.39	0.16	.44	
E10	S03	16.2	-3.6	4.0	65	23									
E10	S01	20.2	-3.0	5.7	115	32	3.7	-3.	2.5	9	0	.22	0.08	.44	
E10	N01	22.6	-3.0	4.5	102	24	4.4	-2.5	2.5	11	-0.5	.20	0.11	.60	
†E10	N02	21.5	-3.2	2.4	52	28									
E10	N03	15.3	-3.0	4.8	73	22	2.1	03.	3.	6	0	0.14	0.08	.63	
†E10	N06	14.9	-4.2	4.7	70	12									
E15	S04	12.9	-3.6	1.9	24	13									add'l line (+20)
E20	S05	9.4	02.9	4.0	38	14									
†E20	S04	9.8	-3.2	2.4	24	14									complex
E20	S03	9.5	-2.8	2.8	27	16									
†E20	N00	12.8	-1.5	3.8	49	20	1.6	-1.5		7	0	0.13	0.15	1.19	complex
†E20	N04	6.3	-2.6	4.8	30	36	2.4	-2.5		16	-0.1		0.52	1.35	1 MHz filters
†E20	N08	< 1.2													1 MHz filters
†E20	N12	3.4	-2.4	3.7	13	10									
E25	S06	13.7	-3.9	1.6	22	18									complex
E25	S04	9.1	-2.6	4.0	36	27									add'l line (+18)
E30	S05	6.9	-2.9	3.3	23	22									add'l line (+18)
†E40	N00	5.2	-2.4	6.5	34	32									
†E40	N08	< 0.6													

† 1973 data

‡ center position at $\alpha 20^h37^m13^s$ $\delta 42°09'$ (1950)

TABLE 2

OBSERVATIONAL PARAMETERS FOR THE CO IN THE +9 km s^{-1} COMPONENT OF THE DR 21–W75 COMPLEX

POSITION FROM CENTER‡		^{12}CO line parameters				^{13}CO line parameters				$V_{12}-V_{13}$	RATIOS ^{13}CO/^{12}CO			NOTES
$\Delta\alpha$	$\Delta\delta$	T_A^*	V_C	ΔV	$T_A^*\cdot\Delta V$	T_A^*	V_C	ΔV	$T_A^*\cdot\Delta V$		T_A^*	$T_A^*\cdot\Delta V$	ΔV	
s	arcmin	K	km/s	km/s	K·km/s	K	km/s	km/s	K·km/s	km/s				
†W40	N00	~ 1.2												
†W40	N08	2.5	6.9	(6.)	15.0									
†W40	N16	8.2	8.2	(4.3)	35.3	2.4	9.7	(6.8)	16.3	-1.5	.29	0.46	1.58	1 MHz filters
†W40	N24	4.6	10.1	(6.0)	27.6									
W30	N18	14.5	12.2	9.0	130.5									
W30	N19	13.7	11.2	5.6	76.7									
W30	N20	14.8	12.1	4.3	63.6									
W25	N17	15.9	10.1	7.4	117.7									
W25	N18	15.5	10.8	9.2	142.6	8.7	10.5	4.2	36.5	0.3	.56	0.26	0.46	
W25	N19	15.0	10.4	5.0	75	6.4	11.	3.5	22.4	-0.6	.43	0.30	0.70	
†W20	S04	5.0	5	(4.5)	22.5									
†W20	N00	9.1	6.1	(4.5)	41.0	2.4	8.3	(5.3)	12.7	-2.2	.26	0.31	1.18	
†W20	N04	14.8	9.5	(7)	103.6	<1					<.07			
†W20	N08	4.9	9.2	(2.3)	11.3	< .5					<.10			
†W20	N12	7.0	8.1	(4.5)	31.5									
†W20	N16	15	8.9	(5)	75.0									
W20	N17	17.8	9.4	4.9	87.2									
W20	N18	13.3	10.8	7.8	103.7	6.4	10.5	3.	19.2	0.3	.48	0.19	0.38	
W20	N19	13.3	10.1	6.0	79.8	4.0	11.	2.5	10	-0.9	.30	0.13	0.42	
†W20	N20	21	11.	(4.5)	97.5									
W15	N17	17.5	9.6	4.6	80.5									
W15	N20	16.4	10.2	7.3	119.7									
W10	S01	4.4	10.2	12.0	52.8	1.7	8.5	3.	5.1	1.7	.30	0.10	0.25	asymetric
W10	N01	3.6	10.2	8.0	28.8	.5	8.1	2.0	1.0	2.1	.14	.03	0.25	asymetric
†W10	N02	10.6	10.	7.2	76.3									asymetric
W10	N03	8.0	10.5	9.0	72.0									asymetric
W10	N05	9.0	9.6	4.8	43.2									
W10	N10	6.3	8.4	4.3	27.1									
W10	N14	9.0	9.4	3.3	27.9									
W08	N18					8.2	11.0	(4.6)						
W05	S02	6.9	7.6	4.8	33.1	<1					<.15			asymetric
W05	S01	4.3	9.0	8.0	34.4	1.2	8.5	4.0	4.8	0.5	.28	.14	0.50	asymetric
W05	N00	6.9	10.2	8.0	55.2	1.6	9.	2.4	3.8	1.2	.35	.07	0.30	asymetric
W05	N01	6.2	9.	7.6	47.1	1.6	9.	2.	3.2	0.8	.22	.08	0.26	asymetric
W05	N02	5.2	10.6	10.2	53.0	.7	8.5	1.	.7	2.1	.13	.01	0.10	asymetric
W05	N03	7.4	8.4	8.4	62.2	1.4	9.	2.7	3.8	-0.6	.19	.06	0.32	asymetric
W05	N04	7.9	8.8	7.1	56.1	1.2	8.5	3.5	4.2	0.3	.15	.07	0.49	asymetric
W05	N05	10.5	9.2	4.0	42.0	1.2	9.	2.	2.4	0.2	.11	.06	0.50	
†E00	S08	12.2	6.9	(4.5)	54.9									
†E00	S04	9.2	6.3	(3.3)	30.7									
E00	S01	6.5	8.4	5.6	36.4	1.0	8.5	3.5	3.5	-0.1	.15	.10	0.63	
‡E00	N00	5.5	9.3	7.0	38.5	2.3	8.5	1.5	3.5	0.8	.42	.09	0.21	
E00	N01	9.2	9.5	7.2	66.2	2.4	8.5	2.	4.8	1.0	.26	.07	0.28	
E00	N02	5.2	10.0	8.4	43.7	1.9	8.	2.5	4.8	2.0	.37	.11	0.30	
E00	N03	5.5	9.4	3.8	20.9	1.0	9.	1.5	1.5	0.4	.18	.07	0.39	
E00	N04	8.1	8.7	2.3	18.6	1.0	9.	1.	1.0	-0.3	.12	.05	0.43	
E00	N05	8.7	9.2	2.2	19.1	.9	9.5	3.	2.7	-0.3	.10	.14	1.36	
†E00	N08	9.1	9.5	(4.4)	40.0	1.4	8.3	(4.5)	6.3	1.2	.15	.16	1.02	
†E00	N12	13.4	8.2	(2.9)	28.9	2.8	9.7	(3.7)	10.4	-1.5	.34	.27	1.28	
†E00	N16	17.7	8.2	(2.5)	44.3	< .5					<.03			
†E00	N20	7.0	11.5	(4.8)	33.6									
†E00	N24	10.6	11.3	(4)	42.4									
E05	S02	6.4	8.0	6.4	41.0	1.0	7.5	2.	2.0	0.5	.16	.05	0.31	
E05	S01	6.2	8.0	4.8	29.8	1.4	8.	3.	4.2	0	.23	.14	0.63	
E05	N00	5.7	8.6	7.2	41.0	2.1	7.5	2.	4.2	1.1	.37	.10	0.28	
E05	N01	7.4	9.5	6.1	45.1	2.1	8.	3.2	6.7	1.5	.28	.15	0.52	
E05	N02	6.9	9.5	5.6	38.6	2.3	8.5	2.5	5.8	1.0	.33	.15	0.45	
E05	N03	8.4	8.8	3.2	26.9	1.6	8.5	2.	3.2	0.3	.19	.12	0.63	
E05	N04	7.6	9.2	2.2	16.7	2.1	9.	3.	6.3	0.2	.28	.38	1.36	
E05	N05	7.7	8.9	2.2	16.9	< .5					<.06			
E10	S03	8.0	6.5	9.7	77.6									
E10	S01	8.0	6.8	7.6	60.8	1.0	7.5	4.	4.0	-0.7	.12	.07	0.53	
E10	N01	9.8	8.4	4.8	45.1	1.9	8.5	3.0	5.7	-0.1	.19	.13	0.63	
†E10	N02	14.9	6.8	(2.4)	35.8									
E10	N03	9.3	8.4	4.0	37.2	1.2	8.5	3.	3.6	-0.1	.13	.10	0.75	
†E10	N06	5.0	8.4	(5.)	25.0									
E15	S04	6.3	7.9	1.0	6.3									add'l line (+20)
E20	S05	3.6	8.0	1.5	5.4									
E20	S04	5.7	7.4	2.0	11.4									complex
E20	S03	5.9	7.6	2.4	14.2									complex
†E20	N00	7.6	6.9	(6.)	45.6	1.0	8.9	(6.5)	6.5	-2.0	.13	.14	1.08	1 MHz filters
†E20	N04	8.7	6.9	(6.5)	56.6	3.0	7.0	(6,5)	19.5	-0.1	.34	.34	1.00	1 MHz filters
†E20	N08	4.3	8.2	(2.4)	10.3									
†E20	N12	618	8.4	(3.5)	23.8									
E25	S06	6.9	8.5	12.0	82.8									complex
E25	S04	7.6	7.7	1.3	9.9									add'l line (+18)
E30	S05	10.7	8.0	4.5	48.2									add'l line (+18)
†E40	N00	12.7	4.8	(6.5)	82.6									
†E40	N08	9.0	8.2	(3.0)	27.0									

† 1973 data

‡ center position at $\alpha 20^h37^m13^s$ $\delta 42^\circ09'$ (1950)

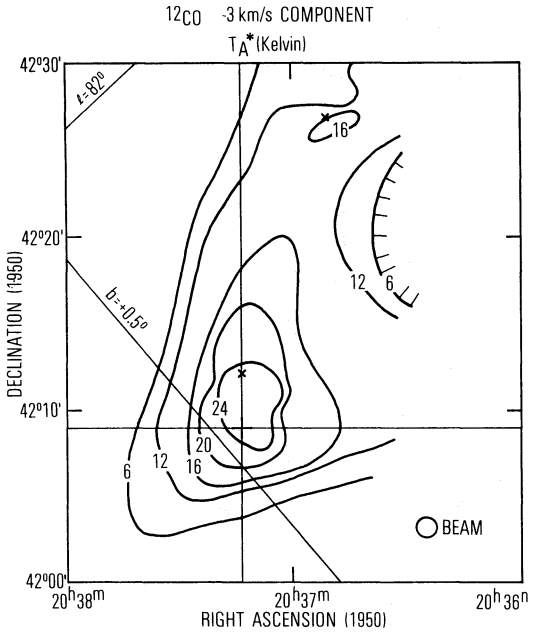

FIG. 2a

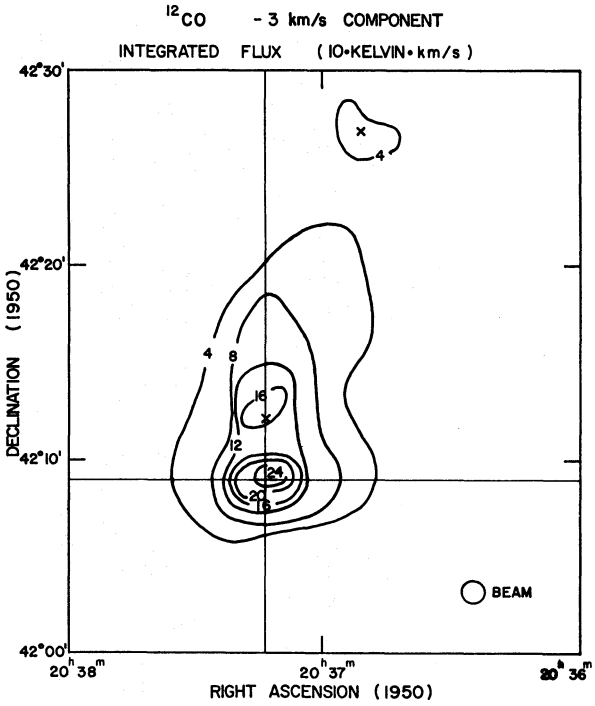

FIG. 2b

FIG. 2.—Distribution of the (*a*) corrected peak antenna temperature T_A^* and (*b*) integrated flux of the ^{12}CO line at a radial velocity of -3 km s^{-1} in the region of DR 21–W75. The three crosses indicate the positions of DR 21 at $\alpha(1950) = 20^h37^m13^s$, $\delta(1950) = 42°08'59''$ (Wynn-Williams 1971); DR 21(OH) at $\alpha(1950) = 20^h37^m13^s$, $\delta(1950) = 42°12'09''$ (Raimond and Eliasson 1969); and W75 N(OH) at $\alpha(1950) = 20^h36^m50^s$, $\delta(1950) = 42°26'58''$ (Hardebeck 1972).

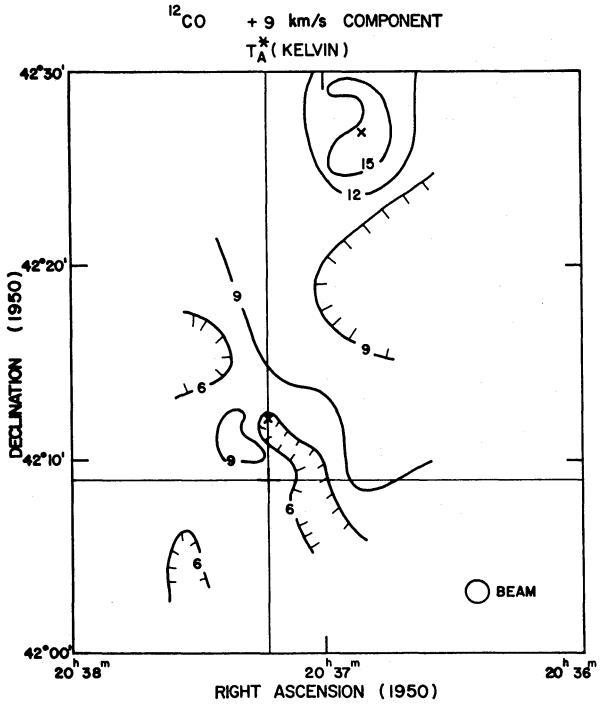

FIG. 3a

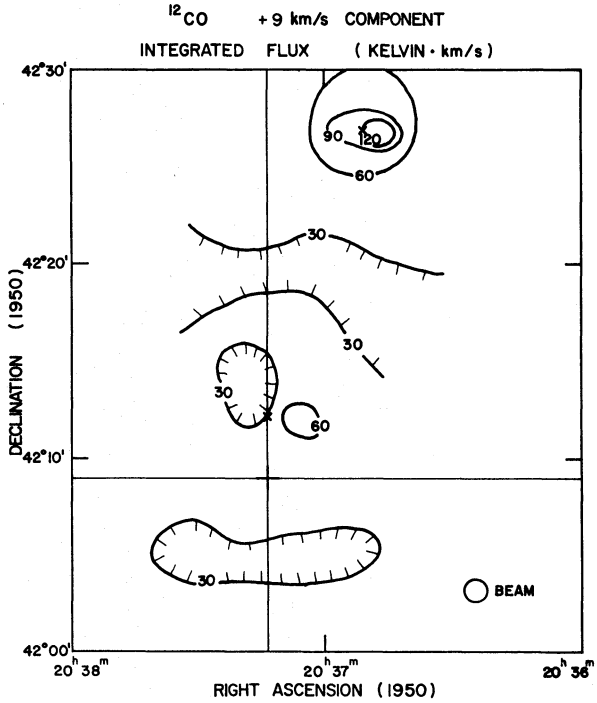

FIG. 3b

FIG. 3.—Distribution of the (*a*) corrected peak antenna temperature T_A^* and (*b*) integrated flux of the ^{12}CO line at a radial velocity near $+9$ km s^{-1} in the region of W75.

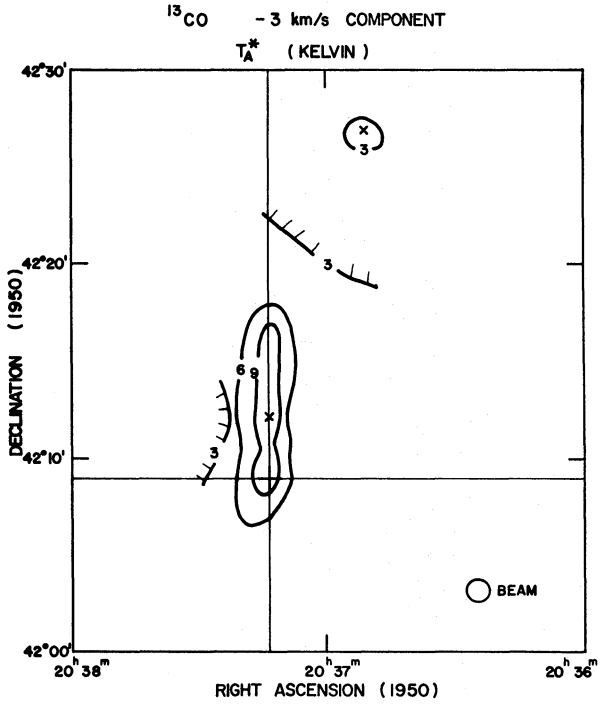

FIG. 4a

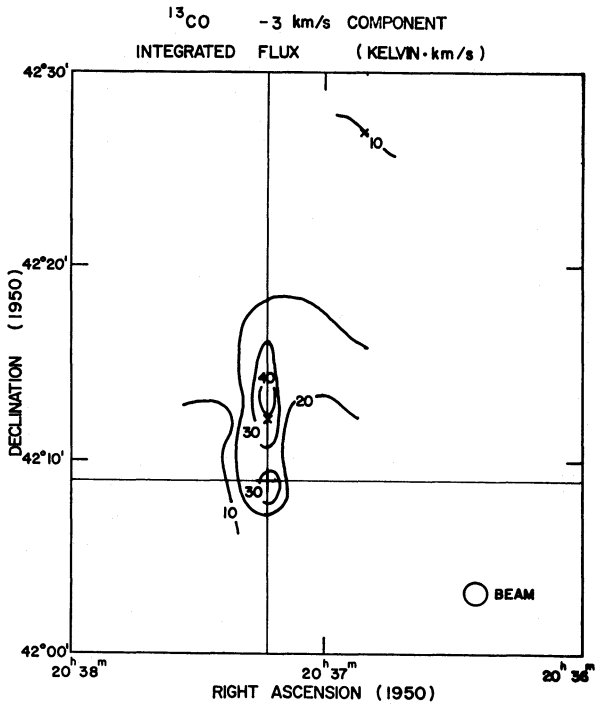

FIG. 4b

FIG. 4.—Distribution of the (*a*) corrected peak antenna temperature T_A^* and (*b*) integrated flux of the ^{13}CO line at a radial velocity of -3 km s^{-1} in the region of DR 21–W75.

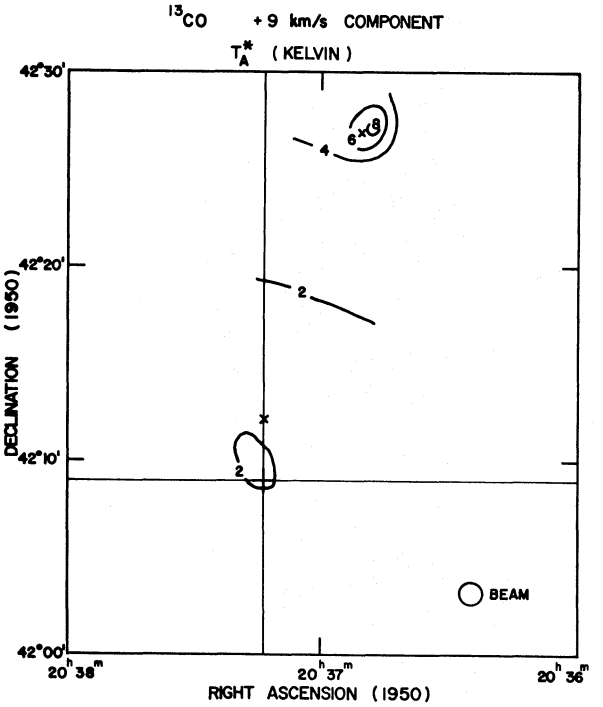

FIG. 5a

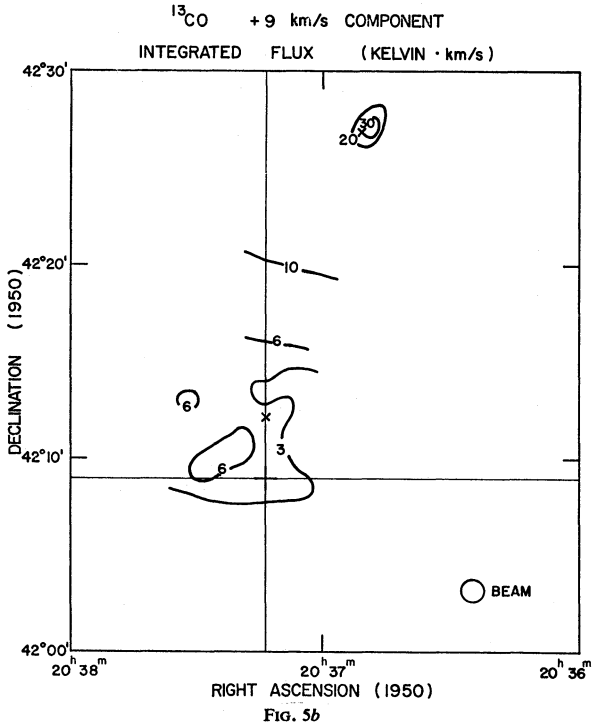

FIG. 5b

FIG. 5.—Distribution of the (*a*) corrected peak antenna temperature T_A^* and (*b*) integrated flux of the ^{13}CO line at a radial velocity near $+9$ km s^{-1} in the region of DR 21–W75.

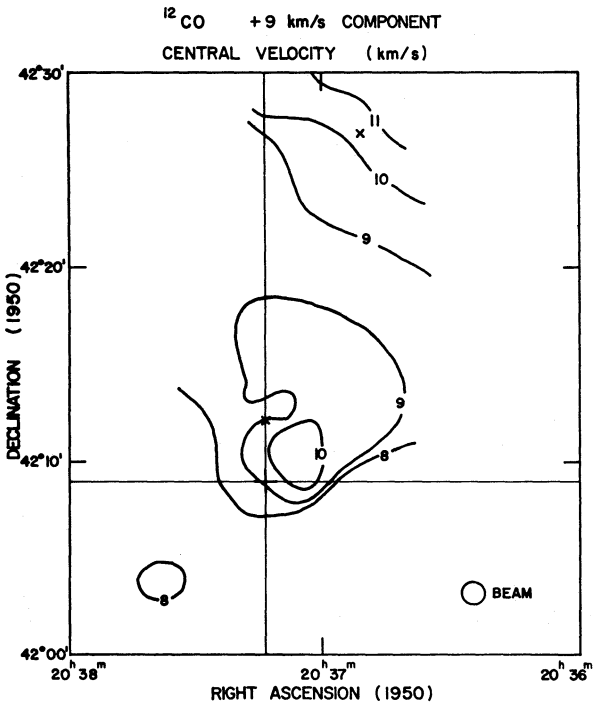

FIG. 6a

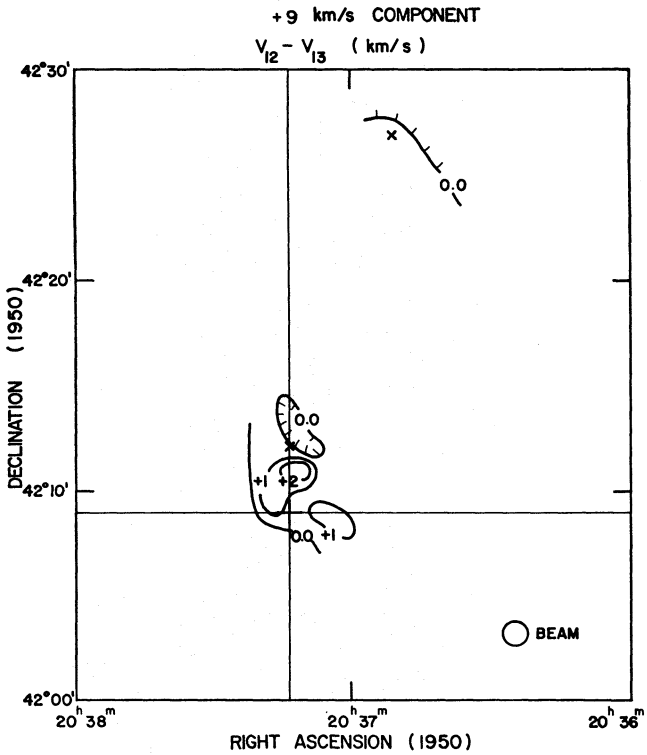

FIG. 6b

FIG. 6.—(*a*) Map of the central velocity of the ^{12}CO line near the average radial velocity of +9 km s^{-1} in the region of DR 21–W75. The values are in km s^{-1} relative to the local standard of rest. (*b*) Map of the velocity difference (km s^{-1}) between the ^{12}CO line and the ^{13}CO line for the +9 km s^{-1} feature.

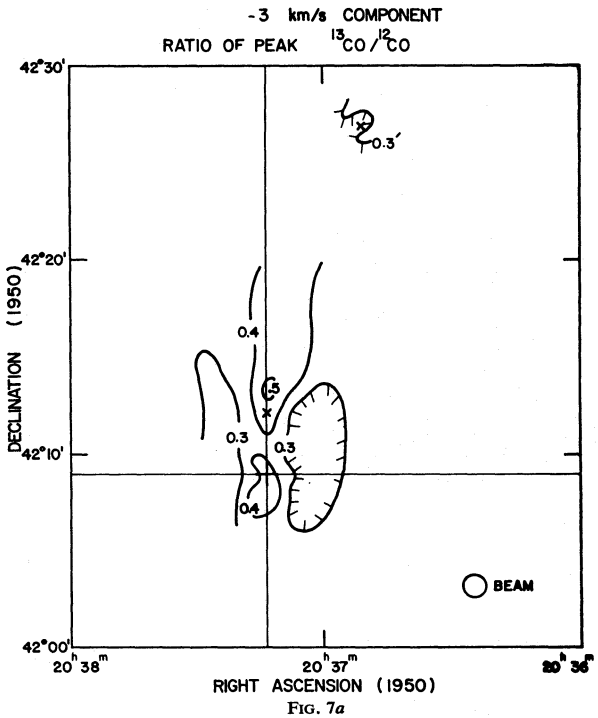

FIG. 7a

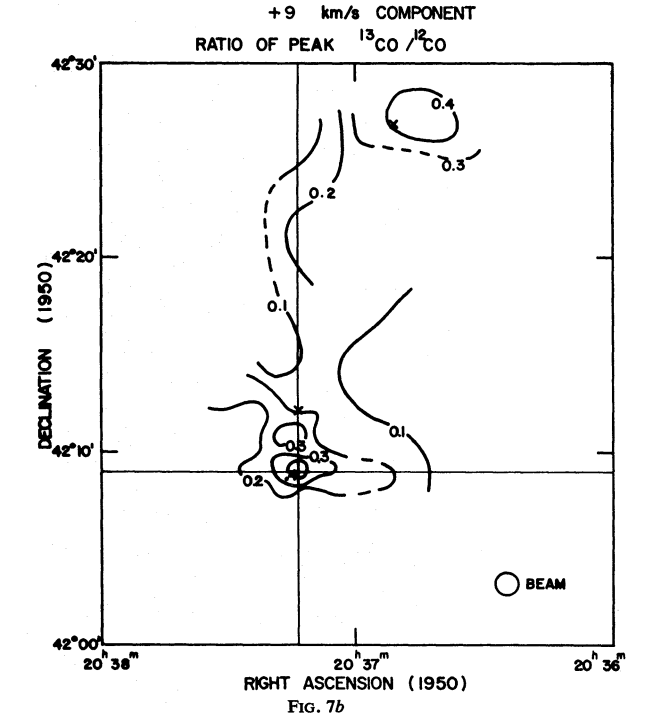

FIG. 7b

FIG. 7.—Map of the ratio of the peak values of $T_A^*(^{13}\text{CO})/T_A^*(^{12}\text{CO})$ in the direction of DR 21–W75 for (*a*) the −3 km s^{-1} velocity component and (*b*) the +9 km s^{-1} component.

does extend northward beyond W75 N (see the maps of T_A* in Fig. 2). The general outline of the cloud producing this line is somewhat elliptical, with a major axis oriented approximately along the line from DR 21 toward W75 N. The feature at +9 km s^{-1} is peaked on W75 N but is also visible throughout the whole complex (Fig. 3). The edges of this component appear to extend beyond the area covered by our data so that the overall shape of the component is not known. It appears reasonable, however, for the purposes of the following discussion, to consider the component to be symmetrically centered on W75 N. The angular separation between the two centers DR 21 and W75 N is about 18′, which, at an assumed distance of 2 kpc (Dickel, Wendker, and Bieritz 1969), corresponds to almost 11 pc. Since the −3 km s^{-1} feature is peaked around the continuum source DR 21, we place DR 21 within that cloud. The other cloud, at +9 km s^{-1}, shows both OH and 6 cm H_2CO absorption and is therefore assumed to lie in front.

Both clouds have irregular features and also significant gradients in brightness from their centers to their edges; but the line of sight at about $20^h37^m02^s$ and 42°18′, midway between the centers of the two clouds, appears to be representative of an average path through each. Therefore, to obtain mean column densities of the molecules within them, we adopted the parameters of each cloud at that position. Using the formulae given in Paper I, we find that, with $T_A(^{12}CO)$ = 16 K, with $T_A(^{13}CO)$ = 3 K, and with a half-power line width of ^{13}CO equal to 3 km s^{-1}, the −3 km s^{-1} component has a ^{13}CO column density of 1.6×10^{16} cm^{-2}. For a $^{13}CO/H_2$ ratio of 2×10^{-6} (Dickman 1976), this corresponds to a column density for molecular hydrogen of 8×10^{21} cm^{-2}. If the cloud is considered to be spherical with a mean radius of 12 pc, then the path length through the cloud at the chosen position is about 20 pc; thus the mean density is ~130 cm^{-3} and the total mass of the cloud is about 4×10^4 $M_\odot$. For the +9 km s^{-1} cloud, the corresponding hydrogen column density is 4×10^{21} cm^{-2}. This cloud is probably somewhat larger; so we adopt a radius of 15 pc to get a mean hydrogen density of ~60 cm^{-3} and a total mass of about 3×10^4 $M_\odot$.

ii) *Relationship with Other Sources and Galactic Structure*

The DR 21–W75 molecular clouds are the most prominent features in this area of Cygnus X. They are ringed to the south by diffuse H II regions seen in the radio continuum (Harten 1978), and the well-known Cyg OB2 association is centered about 1½° to the southwest. The heavy obscuration toward the DR 21–W75 molecular clouds (Dickel and Wendker 1978) indicates that they must lie beyond the Cyg OB2 association at about 2 kpc, but they cannot be much further away or the mean hydrogen densities derived from the observed column densities will become too low to excite the CO. The ^{12}CO temperatures and H_2CO optical depths toward the southern continuum peaks (Seacord and Gottesman 1977) are less than those in the DR 21–W75 complex. The molecular velocities of these other sources are sufficiently different that the detailed relationship, if any, between the DR 21–W75 clouds and the diffuse southern radio sources cannot be determined without further extensive mapping of the molecular emission with both high sensitivity and velocity resolution. The general structures in the continuum, however, do not show any sharp features near or oriented toward DR 21–W75, or any other evidence of an interface between these diffuse clouds and the DR 21–W75 molecular clouds, or between the Cyg OB2 association and the molecular clouds.

One can also consider the possibility that the intensity variations and velocity gradients in the DR 21–W75 clouds are due to their passage through a general spiral shock in the Galaxy. In this case, a velocity gradient across the spiral arm would be expected, with the radial velocity increasing as the galactic longitude increases (Woodward 1976). The velocity gradient in the +9 km s^{-1} component is nearly in the direction of increasing galactic latitude (Fig. 6*a*); so there is no obvious agreement with the model for a galactic shock. Furthermore, recent studies by Lin, Roberts, and Yuan (1978) give no evidence for the presence of a general shock in this part of the Galaxy.

Thus it is difficult to find an external cause, either local or more extended, for the observed structure and dynamics of the DR 21–W75 complex.

iii) *Interrelationship of the Two Clouds*

There are several characteristics of the spectra which suggest that the two clouds are physically near each other rather than a chance superposition on the plane of the sky. First, features at given positions in the maps at one velocity are often evident as hot spots, condensations, or irregularities at the other emission velocity as well. Some of these individual condensations, such as the center of W75 N itself, appear to sufficiently affect the other cloud that it appears more likely they are neighboring rather than chance coincidences on the plane of the sky. These distinct features will be discussed in more detail in § III*b*. Second, the denser of the large clouds has a nearly uniform radial velocity of −3 km s^{-1} everywhere, whereas the other cloud shows a gradient in radial velocity from about +11 km s^{-1} at its suggested center near W75 N down to about +8 km s^{-1} southeast of DR 21 (Fig. 6*a*). This pattern is suggestive of a situation in which the +9 km s^{-1} cloud has been differentially slowed as it passes by the edge of the denser −3 km s^{-1} cloud. A possible geometry of such an interaction is depicted in Figure 8. To obtain the observed velocity gradient in the +9 km s^{-1} cloud for this model, we must place it in front of the −3 km s^{-1} component as shown. Because the region of interaction should cover an area and not a line as viewed by the observer, the somewhat elliptical outline of the −3 km s^{-1} cloud and the straight alignment of high-density features indicated by the ^{13}CO map in Figure 4*a* are not explained by the collision; the orientation may be chance or have some other physical cause. The

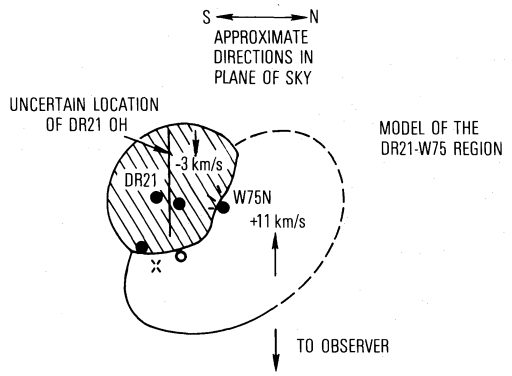

FIG. 8.—Schematic model of the DR 21–W75 region showing a possible configuration of the two large colliding clouds and the various condensations within them. The filled circles represent regions of enhanced temperature and density, the groups of short lines represent heating effects, and the open circle represents a region of increased line width.

velocity gradient in the front cloud (+9 km s^{-1} mean velocity) is most prominent in ^{13}CO (Fig. 6*b*) which is optically thin so that we see deep into the cloud where it has been slowed, whereas in ^{12}CO (Fig. 6*a*) the optical depth is apparently large enough near the direction of DR 21 that we see primarily the front edge where the material has not yet been slowed as much by the collision. Also, in that direction, where the interaction is greatest, we observe a high ^{13}CO/^{12}CO ratio in the +9 km s^{-1} component (Fig. 7*b*), which suggests a possible density enhancement and shock front resulting from the compression. Note that the densities calculated above were for the original, approximately spherical clouds before any collision. After the collision, with the geometry in Figure 8, we find similar densities for both.

Finally, we note the presence of the broad wings in the spectra toward the −3 km s^{-1} cloud which are seen throughout the whole region. Such a profile has not been reported in any other individual molecular cloud complex (e.g., Paper I), except in the CO profiles toward Orion A where it extends less than 0.1 pc from the center (Zuckerman, Kuiper, and Rodriguez Kuiper 1976). We suggest, therefore, that this unusual feature may be related to the interaction of the two clouds. Also related to this is the fact, shown in Figure 1*a*, that neither the ^{12}CO nor the ^{13}CO profile reaches the baseline at all between the −3 km s^{-1} and +9 km s^{-1} components, which suggests that there is gas present at all intermediate velocities, as would be expected from a collision.

In a CO survey of the whole Cygnus X complex with much lower resolution, Cong (1977) suggests that the +9 km s^{-1} cloud may be closer and unrelated to the −3 km s^{-1} cloud, but we find it difficult to reconcile that interpretation with the fine scale heating and velocity gradients observed with the better resolution.

iv) *Broad Wings on the −3 km s^{-1} Line Profiles*

a) *General properties.*—The line profiles in Figure 1 show a significant wing structure which becomes prominent, deviating from a simple Gaussian profile, at a height of about 10% of the peak temperature. If we fit a symmetrical line over the whole spectrum and record the width between points at a level of 1% of the peak height, we obtain a width of 39 km s^{-1}. This is about 3.6 times the half-power width of the line, whereas a Gaussian profile would drop to the 1% level within about 2.6 half-power widths.

Because DR 21 was our reference point for the mapping of the W75 complex, the signal-to-noise ratio is best there, but the wing does appear to be present in both isotopes throughout the region. Adopting the same criterion as mentioned above, we have constructed a map of the distribution of the "wing width" at the 1% level (Fig. 9*a*) which can be compared with the half-power width in Figure 9*b*. It can be seen that the variations in these two parameters do not differ markedly: the typical ratio of wing width to half-power width is between 3 and 6. The reduced signal strength of the ^{13}CO emission makes it harder for one to see the distribution of the wing structure in that species, but it does appear to follow that outlined by the ^{12}CO.

b) *Other molecules.*—The spectrum of the 6 cm formaldehyde line toward DR 21 after removal of a linear baseline is shown in Figure 10*a*. It was obtained using the 43 m telescope of NRAO, which was equipped with a cooled parametric amplifier and has a beamwidth of 6′ at this wavelength. The data from the 413-channel autocorrelation spectrometer have been Hanning smoothed to have an effective resolution of 0.5 km s^{-1}. The two strong lines have velocities of −2.5 and +8.2 km s^{-1} and are in good agreement with the CO lines. The peak continuum temperature of 6.2 K gives optical depths of about 0.33 and 0.08, respectively. The general parameters of the lines are similar to those found by Zuckerman *et al.* (1970), but our improved sensitivity allows detection of the wide velocity wings and of the presence of material at all velocities between the two major components; if inverted, the profile matches almost perfectly that of the ^{13}CO in the same direction. Because the formaldehyde line is seen in absorption, we cannot measure the wings away from the position of the continuum source.

The absorption spectrum of the 1667 MHz OH line toward DR 21 is shown in Figure 10*b*. This was observed with the 36 m telescope of the University of Illinois, which was equipped with a parametric amplifier and 128-channel autocorrelator having an effective resolution of 2.1 km s^{-1}. The profile shows the two components at −2.3 and +8 km s^{-1}, but it also shows a very asymmetric wing structure. Because the 22′ beamwidth of the telescope also covers the OH maser source located 3′ north of the DR 21 continuum (Raimond and Eliasson 1969) with strong emission in the 1665 MHz line at a radial velocity of 0 to +1 km s^{-1} (Goss 1968; Weaver, Dieter, and Williams 1968), there may be some filling in of the profile in Figure 10*b* by material emitting in this velocity range. A possible symmetric wing structure for the −3 km s^{-1} absorption component is shown by the dashed line in Figure 10*b*, assuming the 1667 MHz emission feature as shown.

Finally, W. J. Wilson and M. W. Werner (1978,

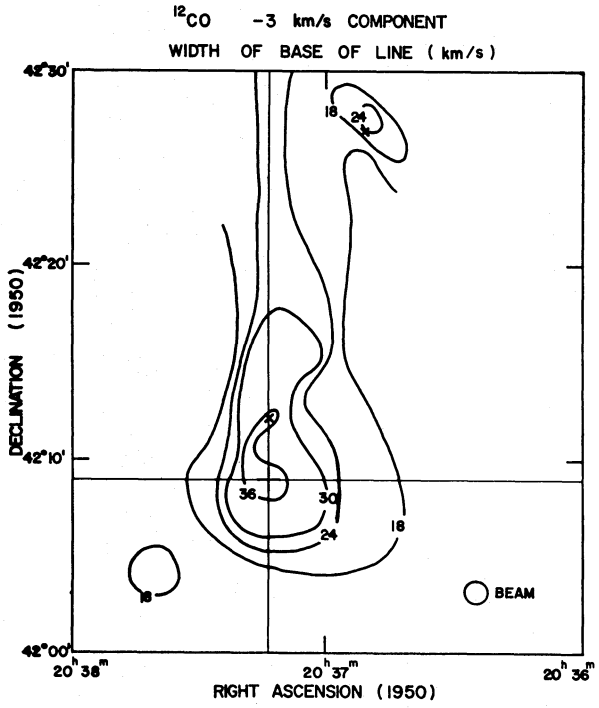

FIG. 9*a*

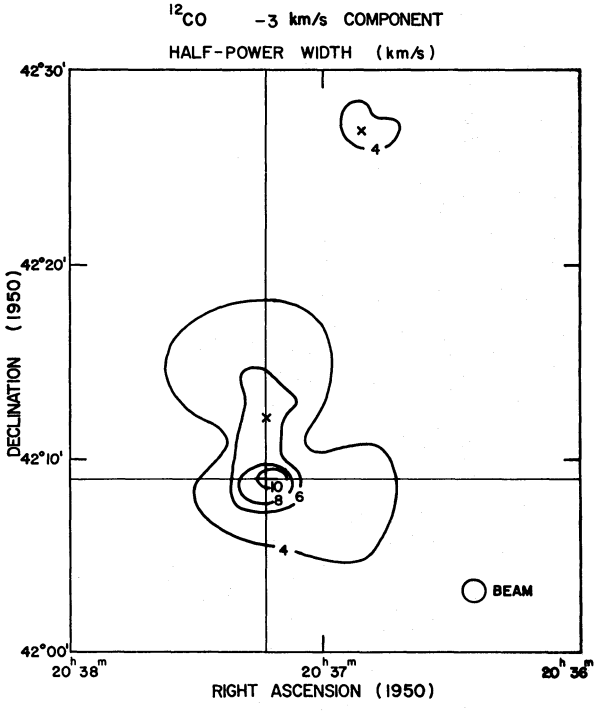

FIG. 9*b*

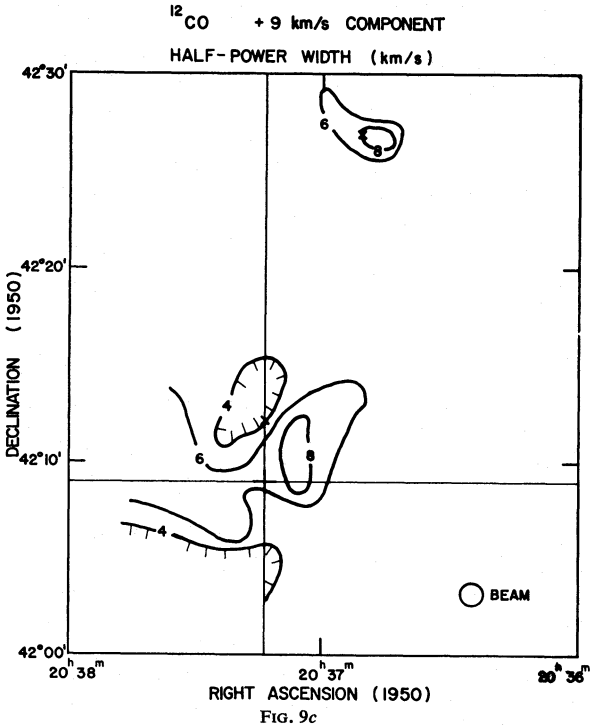

FIG. 9*c*

FIG. 9.—(*a*) Map of the extent of the velocity wings of the ^{12}CO line at -3 km s^{-1} toward the DR 21–W75 complex. The velocities represent the distance in km s^{-1} between the points at a level of 1% of the peak height of the line. (*b*) Map of the width in km s^{-1} at the half-intensity level of the ^{12}CO line at a radial velocity of -3 km s^{-1} in the region of DR 21–W75. (*c*) Map of the width in km s^{-1} at the half-intensity level of the ^{12}CO line at a radial velocity of $+9$ km s^{-1} in the region of DR 21–W75.

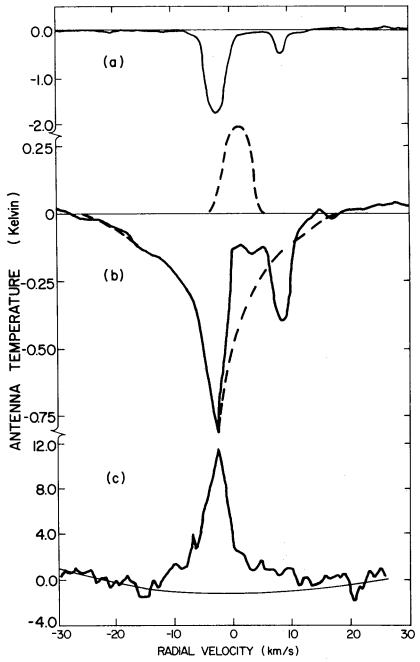

FIG. 10.—Line profiles of molecules toward DR 21: (*a*) 6 cm formaldehyde with a linear baseline removed; (*b*) 1667 MHz OH absorption (the dashed lines represent the fit of a possible emission component at $+1$ km s^{-1} and of a symmetrical absorption line at -3 km s^{-1}); and (*c*) 3 mm CS.

paper in preparation) have observed DR 21 in the 3 mm wavelength transition of CS using the 11 m telescope of NRAO. This spectrum (Fig. 10*c*) is fairly noisy, but there may be a hint of the wide wings.

c) *Discussion.*—As this is the first reported case of such wide wings observed over an extended area of the sky, the phenomenon causing them does not appear to be particularly common but may have interesting astrophysical implications.

If the two clouds are in collision, then a region of significant turbulence and possibly a shock front should exist at their interface, and some of the material should have random motions with speeds up to the space velocity between the two clouds. Only the radial component of their relative motion (~ 14 km s^{-1}) can be measured; but if the observed velocity is a result of such turbulence at the interface, it requires a relative speed between the clouds of 38 km s^{-1}, the total width of the wing feature. Such a large motion is unlikely in view of the observed dispersion of 9 km s^{-1} for the random motions of clouds in the interstellar medium (Mebold 1972). Furthermore, the turbulent material should have the same total spread of velocities everywhere across the interface of the two clouds, whereas we observe a continuous decrease in the line width away from the center of DR 21 (Fig. 9). It is concluded that we are not observing such turbulent material between the clouds.

A different mechanism for producing wide lines is one in which, in the presence of a magnetic field, hydromagnetic oscillations may be set up in the ionized gas within a cloud, and these may couple to the neutral material producing significant nonthermal motion (Arons and Max 1975). It is possible that the proposed collision could create a zone of ionized material in which the waves might grow, but it is difficult to see why the velocity amplitude would not remain constant over the whole face of the clouds rather than taper off near the edges as observed. More information on the ionization fraction and possible magnetic field strength in this region is needed before this mechanism can be investigated further.

Another possible explanation of the wide wings on the -3 km s^{-1} feature is that we are receiving emission from a variety of material along the line of sight in the complicated Cygnus region. The evidence against this is that the wings are broadest near the DR 21 and W75 sources (Fig. 9) and apparently are not present toward other sources in Cygnus X (Seacord and Gottesman 1977). Thus the wings appear to be definitely associated with the DR 21 cloud.

A CO profile with extensive wings has been observed in the direction of the Kleinmann-Low nebula in Orion by Zuckerman, Kuiper, and Rodriguez Kuiper (1976); they suggest that the wings may be attributed to a stellar wind blowing off the newly formed star at the center. The extent of the feature observed by them is less than about 0.1 pc (limited by their resolution); for their estimated mass and velocity, the outflowing material has a total kinetic energy of about 10^{47} ergs, in reasonable agreement with what might be expected from a T Tauri or young O–B star (Herbig 1962; Strom, Strom, and Grasdalen 1975). In the DR 21 case, however, the whole extended cloud (of $4 \times 10^4\ M_\odot$) appears to be participating in the motion; adopting even one-half of the half-width of the Gaussian core of the line (~ 5 km s^{-1}) as a mean velocity, we find a total kinetic energy of greater than 10^{49} ergs. This value approaches that in a supernova and seems unreasonable for outward flow from a star in a cloud with molecular concentrations and a compact H II region in the center.

These considerations suggest that the extended velocity wings may, more likely, represent material which is in collapse. To verify this, the data were compared with models of the region which were calculated using the computer program for the model of a symmetrical cloud written by R. Snell (see the description in Snell and Loren 1977). With this program a cloud model was determined which reproduced the central spectra very well—including the wide wings. The parameters of this model were as follows:

$$T_k = 28\ \mathrm{K} = \text{constant},$$

$$R_{\max} = 12\ \mathrm{pc} = 18',$$

$$V_{\text{collapse}} \propto R,$$

where $V(R = R_{\max}) = 18$ km s^{-1}, and

$$\rho \propto R^{-2},$$

where $\rho(R = R_{\max}/2) = 130\ \mathrm{cm}^{-3}$. T_k is the kinetic

temperature of the cloud, R is the radius, V is the velocity, and ρ is the molecular hydrogen density. The adopted CO/H_2 ratio was 10^{-4}. These numerical values are near the average values determined from the observations above. The basic form of the core-wing profiles can be reproduced with this model, because the collapsing cloud is optically thick in the center but has a sufficiently low density in the outer regions to be optically thin in the higher-velocity wings.

The problem with this model and this technique is that the model is not unique and that computed spectra at other locations in the cloud did not match the observations as well. There are many reasons for this, including the unsymmetrical shape of the cloud, the possibility of a high-density core, and a temperature which probably decreases toward the edge. Models with $V \propto R^{-1}$ or $R^{-1/2}$ did not fit the observations at all and produced self-absorption features; however, models with $V \propto R$ or $R^{1/2}$ fitted the data well. Although such a mode of collapse should apply only to a very young system which has not yet had a chance to "feel" the effect of a density concentration in its center, it is the only model we have found which can reproduce a broad wing structure over an extended area.

The free-fall collapse time for a cloud of this size and density is about 7×10^5 years, and the current collapse velocity should be ~ 12 km s^{-1}, somewhat less than the observed collapse velocity. This significant a collapse is also not seen in cases of single massive clouds (e.g., NGC 6334 [Paper I]; W3 [H. R. Dickel *et al.*, paper in preparation]), so that perhaps the process could be triggered by the collision of this -3 km s^{-1} cloud with the $+9$ km s^{-1} cloud centered on W75 N. The interaction may somehow alter the mass distribution to allow this contraction, and the various irregularities may be caused by the presence of some condensations where young stars are already forming.

b) *Individual Condensations*

Several distinct features appear to be present on the various maps either as peaks in T_A^* or as velocity irregularities. From these, we identify seven regions which probably represent areas of differing physical conditions and of possible star formation in different stages.

i) *DR 21* ($\alpha = 20^h37^m13^s$, $\delta = 42°09'$)

This area which is both an infrared and continuum radio peak (e.g., Rieke *et al.* 1973; Schraml and Mezger 1969), has a high antenna temperature in both ^{12}CO and ^{13}CO as well as broad line widths. These high temperatures and widths are consistent with the existence of a condensation in which stars have already "turned on" and are beginning to heat the gas and dust around themselves sufficiently to create a small H II region complex.

ii) *DR 21*(OH) ($\alpha = 20^h37^m15^s$, $\delta = 42°12'$)

The region of the OH maser appears bright on the CO–temperature maps of the -3 km s^{-1} cloud in Figures 2 and 4, but there is no particular indication of the actual source. The existence of anything at that location is even less apparent on the maps giving velocity information. The OH source probably lies within the -3 km s^{-1} cloud, but we cannot place it better along the line of sight.

iii) *Condensation to the North of DR 21*(OH) ($\alpha \approx 20^h37^m15^s$, $\delta \approx 42°14'$)

This feature, which is prominent on the ratio map of the -3 km s^{-1} temperature in Figure 7*a*, is not particularly significant on the ^{12}CO map (Fig. 2). These data suggest that the region is condensed but is probably not hotter than its surroundings. A tongue of 1 mm continuum emission extending northward into this area from DR 21(OH) (Werner *et al.* 1975) indicates that this is indeed a dusty area which has not evolved far enough to have significantly heated the dust. A somewhat widened half-power width (Fig. 9) also suggests active collapse. Because there is no major effect upon the $+9$ km s^{-1} component at this position and also because the central velocity of this condensation is the same as the -3 km s^{-1} average for the whole cloud, we conclude that the condensation is buried within the large cloud.

iv) *Southeast Condensation* ($\alpha \approx 20^h37^m40^s$, $\delta \approx 42°05'$)

There appears to be an extension of the ^{12}CO contours in Figure 2 to the southeast of the DR 21 peak. The spectra in this vicinity are confused by a velocity component between the two main ones and by another at still higher velocity probably due to other clouds along the line of sight, but it does appear to be a region of possible heating and compression within the -3 km s^{-1} cloud. The intermediate-velocity component suggests that this feature may lie near the interface of the two major clouds. No ^{13}CO data were obtained in this direction; so we cannot obtain further information about the physical conditions there. The feature has apparently not compressed sufficiently to have a noticeable effect upon its surroundings.

v) *W75 N* ($\alpha = 20^h36^m50^s$, $\delta = 42°27'$)

The OH maser W75 N appears to be the dominant source in the extended cloud which was originally moving away from us at 11 km s^{-1}. That it is bright and has broad lines in both ^{12}CO and ^{13}CO suggests both high temperature and high density. It has already formed a star and developed a faint continuum source (Wynn-Williams 1971). Further, the ^{12}CO temperature at this position in the -3 km s^{-1} cloud is high (Fig. 2) but the $^{13}CO/^{12}CO$ ratio (Fig. 7*a*) is low, which suggests that W75 N may produce some heating in the neighboring -3 km s^{-1} cloud but little compression at the interface.

vi) *Eastern Maximum* ($\alpha \approx 20^h37^m20^s$, $\delta \approx 42°11'$)

An additional maximum is seen just to the northeast of DR 21 in both the ^{12}CO and ^{13}CO maps of the $+9$ km s^{-1} component (Figs. 3 and 5). This suggests

an elevated temperature for this feature, but it cannot be very hot or compacted because no increase in infrared emission is seen here (Harvey, Campbell, and Hoffmann 1977). Further, the half-power line width is small (Fig. 9*c*), so any excitation is apparently not produced by turbulence at the interface of the two clouds.

vii) *Western Feature* ($\alpha \approx 20^h37^m05^s$, $\gamma \approx 42°10'$)

To the west of DR 21, however, is a region of increased line width in the $+9$ km s^{-1} cloud (Fig. 9*c*) but with no obvious feature in the T_A* maps (Figs. 3 and 5). The central velocity here is also higher than in the near environs (Fig. 6), so that this may be a region of increased turbulence where the two large clouds interact but where there is yet little heating or compression.

IV. SUMMARY

The DR 21–W75 complex appears to consist of two interacting giant molecular clouds. The denser and more massive of these clouds, centered on DR 21 with a mean radial velocity of -3 km s^{-1}, exhibits broad wings on the line profiles of several molecular species over an extended area. This cloud may have been triggered into an overall collapse. At the center the collapse has proceeded far enough to form stars, which have already created the compact H II region complex DR 21 around them (Harris 1975). Also embedded in this cloud are an OH maser and several other excitation centers in earlier stages of development. The rapid contraction of such a large region is in contrast to the dynamics we observed in the single cloud NGC 6334, where the overall collapse velocity is much less and the embedded sources are more distinct (Paper I). The DR 21 cloud appears to be a young region where the turbulence and outward pressure of the component sources have not developed far enough to retard the contraction.

The space motion of the second cloud in the W75 complex appears to have been differentially retarded as it went past the edge of the denser cloud, so that we observe a gradient in radial velocity from $+11$ km s^{-1} to $+8$ km s^{-1} as we look across the face of the interacting zone. The compact H II region W75 N and nearby OH maser source lie in this $+9$ km s^{-1} cloud, and some other features appear to be developing—possibly under the influence of the interaction with the neighboring cloud.

We thank R. B. Pomphrey for help with the observations and data reduction. We are indebted to J. C. Webber for the OH observations toward DR 21. J. White, M. Hansell, and the Astronomy 305 class at the University of Illinois in the spring semester of 1977 provided assistance with the data analysis. We thank R. Snell for use of his modeling program of the collapsing cloud. We thank A. Seacord and S. Gottesman for making their molecular data of the Cygnus X region available to us before publication. We acknowledge fruitful discussions with R. Harten and P. Woodward. The NRAO is operated by Associated Universities, Inc., under contract with the National Science Foundation. The observations with the 36 m telescope were supported by the Research Board of the University of Illinois. The spectral-line radio astronomy program of the Aerospace Corporation is supported jointly by the National Science Foundation under grant MPS 73-04554 and by the Aerospace Corporate Programs for Research and Investigation. H. R. D. is supported by NSF grants MPS 72-05053 and AST 75-22208 to the University of Illinois. J. R. D. is supported by H. R. D.

REFERENCES

Arons, J., and Max, C. E. 1975, *Ap. J.* (*Letters*), **196**, L77.
Cong, H-i. L. 1977, Ph.D. thesis, Columbia University.
Dickel, H. R., Dickel, J. R., and Wilson, W. J. 1977, *Ap. J.*, **217**, 56 (Paper I).
Dickel, H. R., and Wendker, H. J. 1978, *Astr. Ap.*, in press.
Dickel, H. R., Wendker, H. J., and Bieritz, J. H. 1969, *Astr. Ap.*, **1**, 270.
Dickman, R. L. 1976, Ph.D. thesis, Columbia University.
Downes, D., and Rinehart, R. 1966, *Ap. J.*, **144**, 937.
Goss, W. M. 1968, *Ap. J. Suppl.*, **15**, 131.
Hardebeck, E. G. 1972, *Ap. J.*, **172**, 583.
Harris, S. 1975, in H II *Regions and Related Topics*, ed. T. L. Wilson and D. Downes (Berlin: Springer-Verlag), p. 393.
Harten, R. 1978, in preparation.
Harvey, P. M., Campbell, M. F., and Hoffmann, W. F. 1977, *Ap. J.*, **211**, 786.
Herbig, G. H. 1962, *Adv. Astr. Ap.*, **1**, 47.
Lin, C. C., Roberts, W. W., and Yuan, C. 1978, *Astr. Ap.*, in press.
Mebold, U. 1972, *Astr. Ap.*, **19**, 13.
Morris, M., Palmer, P., Turner, B. E., and Zuckerman, B. 1974, *Ap. J.*, **191**, 349.
Raimond, E., and Eliasson, B. 1969, *Ap. J.*, **155**, 817.
Rieke, G. H., Harper, D. A., Low, F. J., and Armstrong, K. R. 1973, *Ap. J.* (*Letters*), **183**, L67.
Schraml, J., and Mezger, P. G. 1969, *Ap. J.*, **156**, 269.
Seacord, A. W., II, and Gottesman, S. T. 1977, private communication.
Snell, R. L., and Loren, R. B. 1977, *Ap. J.*, **211**, 122.
Strom, S. E., Strom, K. M., and Grasdalen, G. L. 1975, *Ann. Rev. Astr. Ap.*, **13**, 187.
Ulich, B. L., and Haas, R. W. 1976, *Ap. J. Suppl.*, **30**, 247.
Weaver, H., Dieter, N. H., and Williams, D. R. W. 1968, *Ap. J. Suppl.*, **16**, 219.
Werner, M. W., Elias, J. H., Gezari, D. Y., Hauser, M. G., and Westbrook, W. E. 1975, *Ap. J.* (*Letters*), **199**, L185.
Wilson, W. J., Schwartz, P. R., Epstein, E. E., Johnson, W. A., Etcheverry, R. D., Mori, T. T., Berry, G. G., and Dyson, H. B. 1974, *Ap. J.*, **191**, 357.
Woodward, P. R. 1976, *Ap. J.*, **207**, 484.
Wynn-Williams, C. G. 1971, *M.N.R.A.S.*, **151**, 397.
Zuckerman, B., Buhl, D., Palmer, P., and Snyder, L. E. 1970, *Ap. J.*, **160**, 485.
Zuckerman, B., Kuiper, T. B. H., and Rodriguez Kuiper, E. N. 1976, *Ap. J.* (*Letters*), **209**, L137.

Note added in proof.—R. Genzel and D. Downes (1977, *Astr. Ap. Suppl.*, **30**, 145) have detected an H_2O maser W75 S(1) with velocity -3 km s^{-1} which lies within $\frac{1}{2}'$ of our position for a "new condensation" described in

§ III*b*(iii). Further support for our model comes from the observations of E. E. Lekht (1978, *Soviet Astr. Zh.*, **55**, 76) of a weak 1667 MHz OH absorption feature at -3.5 km s^{-1} seen toward W75 N. This suggests that, in Figure 8, a bit of the -3 km s^{-1} cloud should protrude in front of W75 N.

HÉLÈNE R. DICKEL and JOHN R. DICKEL: University of Illinois Observatory, Urbana, IL 61801

WILLIAM J. WILSON: Electronics Research Laboratory, The Aerospace Corporation A6/2457, Box 92957, Los Angeles, CA 90009